

Precise determination of the $2s^22p^5 - 2s2p^6$ transition energy in fluorine-like nickel utilizing a low-lying dielectronic resonance

S. X. Wang,¹ Z. K. Huang,² W. Q. Wen,^{2,3,*} W. L. Ma,¹ H. B. Wang,² S. Schippers,⁴ Z. W. Wu,⁵ Y. S. Kozhedub,⁶ M. Y. Kaygorodov,⁶ A. V. Volotka,⁷ K. Wang,⁸ C. Y. Zhang,⁹ C. Y. Chen,⁹ C. Liu,¹ H. K. Huang,^{2,3} L. Shao,² L. J. Mao,^{2,3} X. M. Ma,² J. Li,² M. T. Tang,² K. M. Yan,² Y. B. Zhou,² Y. J. Yuan,^{2,3} J. C. Yang,^{2,3} S. F. Zhang,^{2,3} X. Ma,^{2,3,†} and L. F. Zhu^{1,‡}

¹Department of Modern Physics, University of Science and Technology of China, Hefei, Anhui 230026, China

²Institute of Modern Physics, Chinese Academy of Sciences, 730000, Lanzhou, China

³University of Chinese Academy of Sciences, 100049, Beijing, China

⁴I. Physikalisches Institut, Justus-Liebig-Universität Gießen, 35392 Giessen, Germany

⁵Key Laboratory of Atomic and Molecular Physics & Functional Materials of Gansu Province, College of Physics and Electronic Engineering, Northwest Normal University, Lanzhou 730070, China

⁶Department of Physics, St. Petersburg State University, Universitetskaya 7/9, 199034 St. Petersburg, Russia

⁷School of Physics and Engineering, ITMO University, Kronverkskiy prospekt 49, 197101 St. Petersburg, Russia

⁸Hebei Key Lab of Optic-Electronic Information and Materials,

The College of Physics Science and Technology, Hebei University, Baoding 071002, China

⁹Shanghai EBIT Laboratory, Institute of Modern Physics, Fudan University, Shanghai 200433, China

(Dated: May 4, 2022)

High precision spectroscopy of the low-lying dielectronic resonances in fluorine-like nickel ions were determined by employing the merged electron-ion beam at the heavy-ion storage ring CSRm. The measured dielectronic resonances are identified by comparing with the most recent relativistic calculation utilizing the FAC code. The first resonance at about 86 meV due to the dielectronic recombination via $(2s2p^6[{}^2S_{1/2}]6s)_{J=1}$ intermediate state was recognized. The experimental determination of the resonance position at 86 meV reaches an uncertainty of 4 meV, which allows precise determination of the $2s^22p^5[{}^2P_{3/2}] \rightarrow 2s2p^6[{}^2S_{1/2}]$ transition energy. The Rydberg binding energy of the 6s electron in the $(2s2p^6[{}^2S_{1/2}]6s)_{J=1}$ state is calculated by the multi-configurational Dirac-Hartree-Fock and stabilization methods. The determined transition energies are $149.056(4)_{\text{exp}}(10)_{\text{theo}}$ and $149.032(4)_{\text{exp}}(6)_{\text{theo}}$, respectively. Moreover, the transition energy has also been calculated by fully relativistic and *ab initio* approaches. Individual theoretical contributions are evaluated by employing the core-Hartree and Kohn-Sham screening potentials, respectively. High-order QED and correlation effects contribute prominently to the total transition energy. The present DR precision spectroscopy study at the CSRm paves the way for future precision measurements of atomic energy levels with heavier highly charged ions.

I. INTRODUCTION

Atomic energy levels of highly charged ions (HCIs) are ideal systems for testing the quantum electrodynamics (QED) and relativistic effects [1–3]. Electron beam ion traps [4, 5] and heavy-ion storage rings [6, 7] have offered unique opportunities for precision studies with HCIs. The applications and QED tests of HCIs have been summarized in the recent reviews [2, 8]. Before Lindroth *et al.* [9] demonstrated the ability of electron-ion recombination resonances near threshold to approach the QED corrections with HCIs, optical spectroscopy was the most commonly used method to test the QED effects [10–13]. In the dielectronic recombination (DR) which is a free electron is resonantly captured into some high Rydberg state with simultaneous excitation of an inner elec-

tron. The formed intermediate autoionization state will be followed by radiative decay to complete the DR process, or by Auger decay back to its original state. Therefore, the associated ionic energies of the doubly-excited states can be approached by analyzing the measured DR resonances. In the doubly-excited states via recombination process, the binding energy of the Rydberg electron can be calculated in the framework of relativistic many-body perturbation theory (RMBPT) with high accuracy [9, 14]. As depicted in FIG. 1, the core excitation energy of the recombining ion can thus be obtained via the conversation law:

$$E_{\text{exc}} = E_{\text{rel}} + E_{\text{bind}}, \quad (1)$$

where E_{exc} is the associated core excitation energy. E_{rel} and E_{bind} are the measured relative collision energy and the calculated Rydberg binding energy, respectively.

Heavy-ion storage ring equipped with an electron cooler serves as an ideal platform to perform the collisional electron-ion recombination experiments [15, 16]. Several storage rings, including the TSR at MPIK in

* wenweiqiang@impcas.ac.cn

† x.ma@impcas.ac.cn

‡ lfzhu@ustc.edu.cn

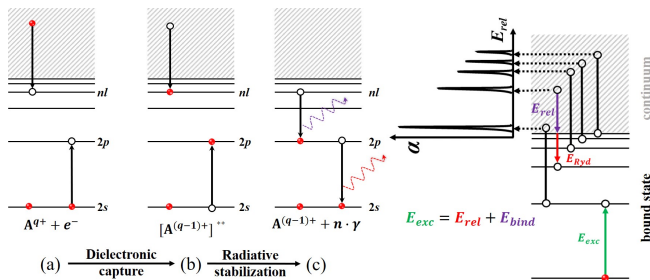


FIG. 1. Schematic diagram of the DR process. (a) \rightarrow (b) is the dielectronic capture: a free electron is resonantly captured into some Rydberg state with simultaneous excitation of an inner electron. (b) \rightarrow (c) is the radiative stabilization: the autoionizing states stabilize via photon emissions. The energy conservation law claims that the core excitation energy equals to the sum of relative collision energy and Rydberg binding energy.

Heidelberg [16], the ESR at GSI in Darmstadt [17] and the CRYRING at MSL in Stockholm [18] have assisted the merged-beam DR experiments. Abundant rate coefficients involving HCIs relevant to astrophysics have been measured at TSR and CRYRING while ESR has been dedicated to the precision studies with heavy HCIs. More recently, HIRFL-CSRm and CSRe at the Institute of Modern Physics (IMP), Chinese Academy of Sciences started contributing to the community [19–25]. With the low-temperature electron target and the merged-beam technique, the experimental resolution could be improved prominently, in particular for the low-lying resonances above the threshold [9, 14]. The $4p_{1/2} \rightarrow 4s_{1/2}$ energy splitting in copper-like Pb^{53+} ion was determined by analyzing the sub-meV resonances with an accuracy of 1 meV, corresponding to a precision of 8.5 ppm [9]. The subsequent experiments with lithium-like Kr^{33+} and Sc^{18+} ions were done at the CRYRING and TSR, respectively. The energy splitting of $2s_{1/2} - 2p_{1/2}$ of Kr^{33+} and $2s_{1/2} - 2p_{3/2}$ of Sc^{18+} were determined with an accuracy of several meV [26, 27]. With the commissioning of an extra ultracold photocathode electron target, Lestinsky *et al.* [14] improved the accuracy of the $2s_{1/2} - 2p_{3/2}$ energy splitting in Sc^{18+} by an order of magnitude. Furthermore, the hyperfine structure was resolved and the screened radiative corrections were tested. The following attempts with multi-electron beryllium-like Ge^{28+} and boron-like Fe^{21+} ions have also been done at the TSR with the photocathode electron target [28, 29]. However, the many-body expansion in multi-electron systems could be quite different from the cases in lithium-like cores. The associated transition energies are still not available due to the lack of an accurate calculation of the Rydberg binding energies in the recombined ions [28, 29]. Another method to determine the transition energy using the DR spectroscopy refers to an extrapolation of the Rydberg resonance series to the limit of $n \rightarrow \infty$ [30, 31].

Here, we present a precision spectroscopy measurement

with a more complex system of fluorine-like $^{58}\text{Ni}^{19+}$. By employing the merged-beam technique at the CSRm, we have measured the dielectronic recombination rate coefficients for $^{58}\text{Ni}^{19+}$ ions in the energy of 0-160 eV, including all of the resonances associated with $\Delta N = 0$ core excitations [22]:

$$^{58}\text{Ni}^{19+}(2s^22p^5[{}^2P_{3/2}]) + e^- \rightarrow \begin{cases} ^{58}\text{Ni}^{19+}(2s^22p^5[{}^2P_{1/2}]nl)^{**} \rightarrow ^{58}\text{Ni}^{18+} + \gamma; \\ ^{58}\text{Ni}^{19+}(2s2p^6[{}^2S_{1/2}]nl)^{**} \rightarrow ^{58}\text{Ni}^{18+} + \gamma. \end{cases} \quad (2)$$

The intermediate states of the measured DR resonances have been identified by comparing the experimental result with the theoretical calculation utilizing the Flexible Atomic Code (FAC) [32]. The first resonance via the $(2s2p^6[{}^2S_{1/2}]6s)_{J=1}$ state at very low collision energy could be determined very precisely. Thus, our measurement of the low-lying DR resonance bears a potential to determine the associated $2s^22p^5[{}^2P_{3/2}] \rightarrow 2s2p^6[{}^2S_{1/2}]$ transition energy with an uncertainty of several meV as long as the Rydberg binding energy of the $6s$ electron could be evaluated with an accuracy at the same level. Note that the electron correlation effects in many-electron systems usually restrict the QED tests. The *ab initio* QED calculated transition energy with individual theoretical contributions offers an opportunity for QED test in fluorine-like nickel.

Knowledge of the $2s^22p^5[{}^2P_{3/2}] \rightarrow 2s2p^6[{}^2S_{1/2}]$ transition in fluorine-like nickel is important not only for atomic physics but also for diagnostics in fusion science and astrophysics. The first observations of this transition were reported by Doschek *et al.* [33] in a laser produced plasma and by Breton *et al.* [34] in a tokamak plasma with an uncertainty of 36 meV. A later measurement by Sugar *et al.* [35] in the TEXT tokamak reduced the uncertainty to 9 meV. In addition, various theoretical methods have been applied to evaluate this transition energy, such as the many-body perturbation theory (MBPT) [36, 37], the multi-configuration Dirac-Hartree-Fock (MCDHF) method [37, 38], the relativistic distorted-wave (RDW) method [39] and an all-order perturbative method [40]. It should be stressed that the electron correlation effect makes a significant contribution to the transition energy, while the correlations were not considered completely in most of the theoretical calculations. The discrepancies between these calculated data and the experimental measurements could be as high as 1% [39, 40]. Based on these observations and calculations, the NIST recommended value for this transition energy is now 149.05 ± 0.12 eV [41]. Therefore, benchmark experimental measurement with an improved accuracy is important not only for cross-checking with previous plasma observations but also for testing different theoretical models as well as the correlation effect.

The paper is organized as follow. The experimental procedure is presented in Sec. II with the detailed discussion of the data reduction and error analysis. In Sec. III, we present a general description of the theoretical

treatment. The experimental results are then discussed in Sec. IV. Finally, a general summary is concluded in Sec. V.

II. EXPERIMENTS AND DATA ANALYSIS

A. Experimental measurement

The experiment was performed by employing the merged-beam technique at the heavy-ion storage ring CSRm at the Institute of Modern Physics in Lanzhou, China. Several DR measurements related to astrophysical and plasma applications have been carried out successfully at the CSRm [20–24, 42–46] since the calibration experiment with lithium-like Ar¹⁵⁺ in 2015 [19]. Recombination rate coefficients of fluorine-like nickel have also been published previously [22]. Here we will focus on the precision studies with the low-lying DR resonances.

In the present measurement, the ⁵⁸Ni¹⁹⁺ ion beam from a superconducting electron cyclotron resonance ion source [47] was accelerated by a sector focused cyclotron and then injected into the storage ring at an energy of 6.15 MeV/u. The stored ion beam reached a maximum current of 80 μA after the injection pulses, corresponding to 3.7×10^8 stored ions. The circulating ion beam will pass through the electron-ion interaction region with an effective length of 4.0 m millions of times per second. The electron beam from the cathode are confined by the magnetic field to overcome the space-charge effect. The magnetic fields at the cathode and the cooler section are 125 mT and 39 mT, respectively. The transverse electron beam energy spread is reduced by adiabatically passing from the high magnetic field in the cathode to a lower magnetic field in the cooler section [48]. The expanded electron beam with a diameter of 62 mm and density of $7.1 \times 10^6 \text{ cm}^{-3}$ was achieved in the interaction region. The longitudinal energy spread were largely reduced by accelerating the beam energy to the desired cooling condition and the final electron beam velocity distribution in the cooler section can be expressed as [49]

$$f(\vec{v}, v_0) = \left(\frac{m_e}{2\pi kT_{\parallel}}\right)^{1/2} \exp\left[-\frac{m_e(v_{\parallel} - v_0)^2}{2kT_{\parallel}}\right] \times \frac{m_e}{2\pi kT_{\perp}} \exp\left(-\frac{m_e v_{\perp}^2}{2kT_{\perp}}\right), \quad (3)$$

where kT_{\parallel} and kT_{\perp} are the longitudinal and perpendicular electron temperatures. The distribution is regarded as a flattened Maxwellian due to the fact that $kT_{\parallel} \ll kT_{\perp}$. v_0 corresponds to the energy detuning applied to the electron beam. v_{\parallel} and v_{\perp} are the longitudinal and perpendicular components of the electron velocity \vec{v} . The electron beam profile was controlled by changing the ratio of the applied voltages at the control and anode electrodes [50]. A uniform beam density distribution was achieved in the present measurement.

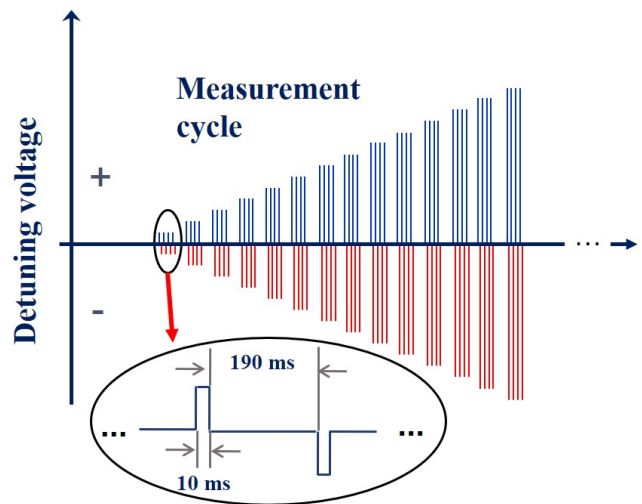


FIG. 2. Illustration of the detuning mode in the present measurement. The data recording was processed volt by volt, i.e., we only measured the recombined ions for a single detuning voltage in each injection cycle to achieve enough statistical counts.

The injected ion beam was cooled down by merging with the cold electrons via Coulomb interaction [51]. Then the stored ion beam intensity could be enhanced by orders of magnitude after accumulation. In the cooling condition, the electrons and ions shared the same average velocity in the laboratory frame, corresponding to zero electron-ion collision energy in the center-of-mass frame. The cold electrons can also act as an electron target by detuning the electron beam energy and the measurements of electron-ion collisions at non-zero energies were available. Before data taking, the ion beam was first electron-cooled for about two seconds after the injection pulses. During the measurement cycle, the electron beam energy was controlled by a designed detuning system, i.e., switched quickly between the cooling point and positive or negative detuning voltages as illustrated in FIG. 2. After every 10 ms of detuning, the ion beam was cooled down for another 190 ms to keep the beam quality. The recombined ions with a changed charge state were separated from the primary ion beam in the dipole magnet downstream from the electron cooler and detected by a movable scintillation particle detector (YAP: Ce+PMT) with a nearly 100% efficiency [52]. A sketch view of the electron cooler and the particle detector is presented in FIG. 3. The ion beam current and the revolution frequency were monitored by a DC current transformer and a Schottky spectrum [53], respectively.

B. Data reduction

The absolute recombination rate coefficients were obtained by normalizing the recorded counting rates $R(E)$

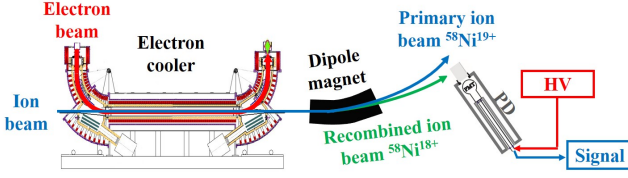


FIG. 3. Schematic view of the CSRm electron cooler. The scintillation particle detector was placed behind the dipole magnet downstream the electron cooler to stop and count the recombined ions.

to the electron and ion beam currents [54]:

$$\alpha(E) = \frac{R(E)}{N_i n_e (1 - \beta_e \beta_i)} \frac{C}{L}, \quad (4)$$

where N_i and n_e are the number of the stored ions and the electron beam density, respectively. $C = 161.0$ m and $L = 4.0$ m are the circumference of the ring and the effective interaction length. β_e and β_i are the velocity factors of the electron and ion beams, respectively.

In every measurement cycle, the recombined ion counts for a single detuning voltage was recorded. Positive and negative detuning voltages were applied in turns for 10 ms. The recombined ion counts and the related parameters were recorded by millisecond and the recorded data in the middle of detuning periods were taken to derive the rate coefficients in the data processing. The original spectra of the ion counts as a function of the detuning voltages up to ± 150 V is presented FIG. 4 (a).

The electron-ion relative collision energy in the center-of-mass-frame is given by:

$$E_{\text{rel}} = m_i c^2 (1 + \mu) \cdot \left[\sqrt{1 + \frac{2\mu}{(1 + \mu)^2} (G - 1)} - 1 \right], \quad (5)$$

with $\mu = m_e/m_i$ is the electron-ion mass ratio and

$$G = \gamma_e \gamma_i - \sqrt{(\gamma_e^2 - 1)(\gamma_i^2 - 1)} \cos \theta. \quad (6)$$

Here, γ_e and γ_i are the corresponding Lorentzian factors of electron and ion beams. θ is the angle between the two beams in the laboratory frame. The resulting experimental energy resolution for the measured resonances with the electron cooler in a storage ring can be expressed as:

$$\Delta E(E_{\text{rel}}) = \sqrt{(\ln 2 \cdot k_B T_{\perp})^2 + 16 \ln 2 \cdot k_B T_{\parallel} \cdot E_{\text{rel}}}. \quad (7)$$

It is clear that the low-energy resonances can be determined with the highest resolution.

By transforming the detuning voltages into the relative collision energies and the counting rates into the rate coefficients, we have got the recombination spectra of the rate coefficients as a function of the collision energies as presented in FIG. 4 (b). It should be noted that the ion counts via radiative recombination (RR) and charge exchange with the residual gases were also recorded. Thus

the obtained rate coefficient spectra featured as several isolated DR peaks over a damped RR continuum and a linear background. The RR enhancement around zero collision energies resulted in a huge rate coefficient near the threshold [46, 55, 56].

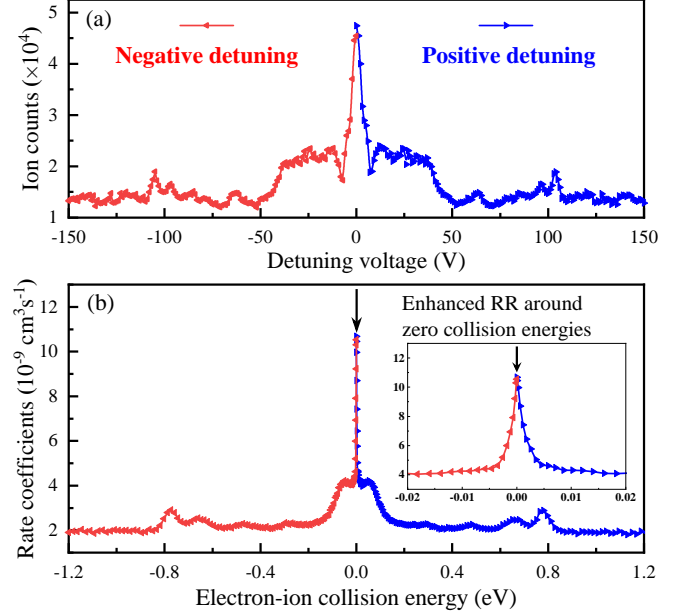


FIG. 4. (a) The original recorded recombined ion counts along with the detuning voltages up to ± 150 V. (b) The derived rate coefficients as a function of the electron-ion collision energy in the range of 0-1.2 eV, corresponding to the detuning voltages up to ± 150 V. Noting that the collision energies for negative detuning voltages are marked by a negative sign. The inset highlights the enhanced RR rate coefficients above the threshold.

The DR spectrum of $^{58}\text{Ni}^{19+}$ ions in the energy range of 0-14 eV is presented in FIG. 5. The calculated DR cross sections are convoluted with the experimental electron beam velocity distribution to compare with the measured rate coefficients. The most recent calculation by the FAC code is found in a good agreement with the measured data. The minor discrepancies could be attributed to the electron correlation effects which are not able to be considered completely in the calculation. The inset enlarges the low-energy resonances below 1 eV and the vertical bars are the calculated positions for the corresponding resonances as marked. Recombination via the $2s2p^6[{}^2S_{1/2}]6s$ and $2s^22p^5[{}^2P_{1/2}]17l$ states are the dominant channels in this energy range. Due to the limited experimental resolution, the fine structures are not well-resolved in the present measurement. The only isolated resonance at around 80 meV is attributed to the recombination via the $(2s2p^6[{}^2S_{1/2}]6s)_{J=1}$ intermediate state.

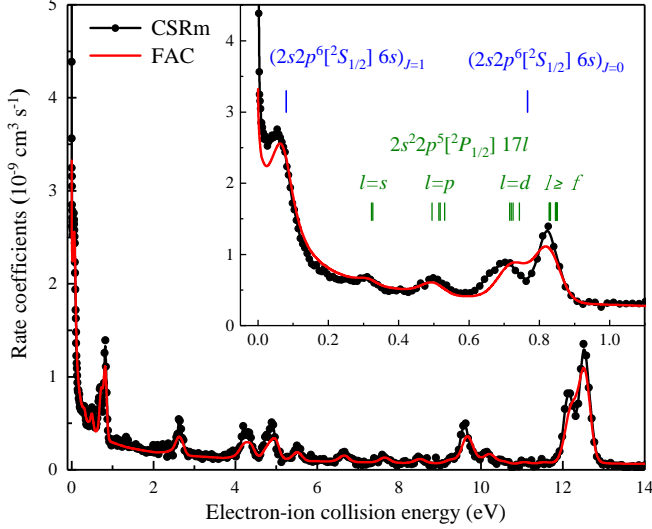


FIG. 5. The measured DR spectroscopy in comparison with the most recent theoretical calculation at low collision energies. The dotted-connected line is the experimental data while the red solid line is the FAC calculation. The inset enlarges the low-energy resonances with the calculated resonance positions indicated by the vertical bars.

C. Error analysis

According to Eq. (5), the accuracy on the determination of the collision energy depends on the measurements of the Lorentzian factors of the electron and ion beams as well as the colliding angles between the two beams. The experimental uncertainty due to the tiny colliding angle θ on the factor G can be written as:

$$\begin{aligned} \delta G_\theta &= \sqrt{(\gamma_e^2 - 1)(\gamma_i^2 - 1)} \cdot 2 \sin^2 \frac{\theta}{2} \\ &\approx \frac{\sqrt{(\gamma_e^2 - 1)(\gamma_i^2 - 1)} \cdot \theta^2}{2} \end{aligned} \quad (8)$$

The Lorentzian factor of the electron beam can be calculated via:

$$\gamma_e = 1 + \frac{e(U_{\text{cath}} + U_{\text{detuning}} + U_{\text{sp}})}{m_e c^2}, \quad (9)$$

where U_{cath} is the electron cathode voltage at the cooling condition. U_{detuning} is the applied detuning voltage at non-zero collision energies. U_{sp} is the corresponding space-charge potential. With the corrections including the influences by the ion beam, the space charge potential in the center of the electron beam for the CSRm electron cooler can be expressed as:

$$U_{\text{sp}}(r) = -(1 - \xi) \frac{I_e}{4\pi\epsilon v_0} \left[1 + 2 \ln \frac{r_{\text{tube}}}{r_{\text{ebeam}}} \right], \quad (10)$$

where $\xi = 0.07$ is the correction factor. I_e and v_0 are the electron beam current and velocity, respectively. ϵ is the vacuum permittivity. r_{tube} and r_{ebeam} are the beam

tube radius and the electron beam radius, respectively. The Lorentzian factor of the ion beam can be calculated via:

$$\gamma_i = 1 + \frac{E_{\text{ion}}}{m_u c^2}, \quad (11)$$

with m_u is the atomic mass.

The resulted uncertainty due to the space charge effect mainly comes from the position of the ion beam in the electron beam. It should be noted that the cathode voltage applied to the electron cooling system was not calibrated in an absolute scale, the electron beam energy was calculated with the space charge effect taken into account to match the ion beam energy at the cooling condition. Since the collision energy depends monotonically on the ion beam energy, the corresponding uncertainties due to the ion beam energy are calculated with the lower and upper limit through

$$\delta E_{\text{ion}} = \frac{1}{2} \left| E_{\text{col}}(E_{\text{ion}}^{\text{upper limit}}) - E_{\text{col}}(E_{\text{ion}}^{\text{lower limit}}) \right|. \quad (12)$$

Here, the ion beam energy was determined by the magnetic rigidity with an uncertainty of 0.5%. Both the uncertainties in γ_i and U_{cath} are included in δE_{ion} .

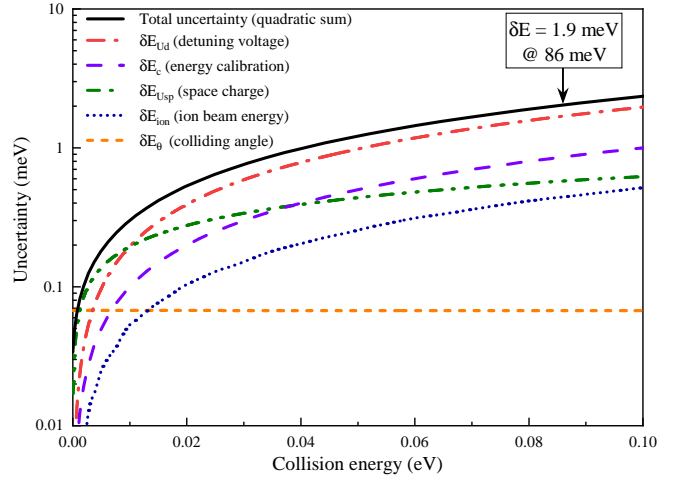


FIG. 6. Systematical uncertainties on the determination of the collision energies. The total uncertainty (without drag force shift and the fitting errors taken into account) for the first resonance at 86 meV is about 1.9 meV.

The maximum relative uncertainty of the applied detuning voltage was at most 2%. The remaining error due to the extra space-charge effect caused by the detuning voltage is also taken into account. It should be noted that the absolute energy scale was multiplied by a factor of 0.98 to match the known $2s2p^6[^2S_{1/2}]nl$ series limit. An error of 1% was introduced due to the energy calibration. All of the above mentioned uncertainties as a function of the collision energies are presented in FIG. 6.

During the measurement period, detuning voltages were applied to the electron beam to achieve nonzero

TABLE I. Experimental uncertainties on the determination of first resonance at 86 meV.

	$\delta E_{c.m.}^{(exp.)}$ (meV)
Colliding angles	0.1
Detuning voltage	1.6
Space charge effect	0.5
Ion beam energy	0.4
Energy calibration	0.9
Drag force effect	0.5
Total (quadratic sum)	2.0

collision energies. The Coulomb interaction between the electron and ion beams yielded a drag force on the ion beam, trying to pull them to the current electron beam velocity [27, 57]. However, the drag force effect could be minimized under the present measurement modes, i.e., the detuning voltages were fast switched between the positive and negative values with a long cooling period between them. The energy shift caused by the drag force effect in the present experiment could be less than 0.5 meV for the determination of the first resonance at 86 meV. The absolute systematical uncertainties on the determination of the first resonance at 86 meV are listed in TABLE I. A total experimental uncertainty of 2 meV is finally achieved.

III. THEORETICAL TREATMENT

A. MCDHF calculation

The $2s^22p^5[{}^2P_{3/2}] \rightarrow 2s2p^6[{}^2S_{1/2}]$ transition energy and the binding energy of the $6s$ electron in the $2s2p^6[{}^2S_{1/2}]6s$ state are calculated by using the relativistic atomic structure package GRASP2018 [58], which was developed based on the multi-configurational Dirac-Hartree-Fock (MCDHF) method [59, 60]. In this method, an atomic-state wavefunction with a specific parity P , total angular momentum J , and its projection M on the quantization axis is approximated by a set of configuration-state wavefunctions (CSFs) with the same PJM as follows [59, 60],

$$\psi_{\alpha}(PJM) = \sum_{r=1}^{n_c} c_r(\alpha) |\phi_r(PJM)\rangle. \quad (13)$$

Here, n_c is the number of the CSFs used. $c_r(\alpha)$ denotes configuration mixing coefficients, which give rise to a representation of the atomic state $|\psi_{\alpha}\rangle$ in the chosen basis $\{|\phi_r\rangle\}$. The CSFs are initially generated as an anti-symmetrized product of a set of orthonormal orbitals and, then, optimized self-consistently in the basis of the Dirac-Coulomb-Breit Hamiltonian, which is followed by an inclusion of the quantum-electrodynamical effects into the representation $c_r(\alpha)$ of the atomic state $|\psi_{\alpha}\rangle$ by diagonalizing the Dirac-Coulomb-Breit Hamil-

tonian matrix. In the calculations of the excitation energy from $2s^22p^5[{}^2P_{3/2}]$ to $2s2p^6[{}^2S_{1/2}]$ in fluorine-like Ni^{19+} ion, all the single and double substitutions from the multi-reference (MR) configurations (the $2s^22p^5$, $2s2p^6$, $2s^22p^43p$, and $2s2p^53p$) to the active set $\{9s, 9p, 9d, 9f, 9g, 9h, 9i, 9k\}$ are considered, which generate 686327 CSFs for the block of $J = 3/2$ and odd parity, and 274090 CSFs for the block of $J = 1/2$ and even parity, respectively. Moreover, in obtaining the energy level $(2s2p^6[{}^2S_{1/2}]6s)_{J=1}$ of neon-like Ni^{18+} ion, all the single and double substitutions from the MR configurations (the $2s2p^65s$, $2s2p^66s$, and $2s2p^67s$) to the active set $\{13s, 13p, 13d, 13f, 13g, 12h, 11i, 10k\}$ are considered, which generate 522644 CSFs for the block of $J = 1$ and even parity.

In Table II, total energies (E_n) of the $2s^22p^5[{}^2P_{3/2}]$ and $2s2p^6[{}^2S_{1/2}]$ levels of fluorine-like Ni^{19+} ion and the $(2s2p^6[{}^2S_{1/2}]6s)_{J=1}$ level of neon-like Ni^{18+} ion are presented as a function of the increasing active set (AS), as well as the transition energies ΔE (eV) for the transitions $2s2p^6[{}^2S_{1/2}] \rightarrow 2s^22p^5[{}^2P_{3/2}]$ and $(2s2p^6[{}^2S_{1/2}]6s)_{J=1} \rightarrow 2s2p^6[{}^2S_{1/2}]$. The MCDHF calculated total energies and ΔE are well converged with respect to the increasing size of the AS.

B. Ab initio calculation

Different theoretical approaches, e.g., complex coordinate rotation method [61], Feshbach projection operator method, optical potential method, R -matrix method, etc. (see, e.g., Ref. [62] and references therein) have been proposed to describe the autoionizing states. In the present work, we apply the stabilization method (SM), pioneered by Hazi and co-workers [63, 64] utilized in numerous investigations [65–68]. The idea of this method [69] is to diagonalize the Hamiltonian of a quantum system with suitable square-integrable real wave functions and investigate the spectra in the neighborhood of resonance position under small variations of the basis set. It can be done elegantly using the spectral density of states function

$$\rho_n(E) = \left| \frac{\xi_{i+1} - \xi_i}{E_n(\xi_{i+1}) - E_n(\xi_i)} \right|, \quad (14)$$

where ξ_i is the basis variation parameter, $E_n(\xi_i)$ is the energy level near the resonance position. The maximum of the spectra density function ρ_n corresponds to the energy of resonance state (see, e.g., Ref. [68] for details). Our realization of the approach is based on the CI-DFS method, where the basis set is varied by the reference energy parameter for Sturm basis orbitals.

The QED calculations of the transition $2s2p^62S_{1/2} \rightarrow 2s^22p^52P_{3/2}$ energy in fluorine-like nickel is based on the QED perturbation theory in the extended Furry picture [70], which previously was also employed for the evaluation of the ground state fine structure energy in fluorine-like ions [71–74]. The zero-order Hamiltonian is defined

TABLE II. Total energies (E_h) of the $2s^22p^5 [^2P_{3/2}]$ and $2s2p^6 [^2S_{1/2}]$ levels of fluorine-like Ni^{19+} ion and the $(2s2p^6 [^2S_{1/2}]6s)_{J=1}$ level of neon-like Ni^{18+} ion are presented as a function of the increasing active set (AS), as well as the transition energies ΔE (eV) for the transitions $2s2p^6 [^2S_{1/2}] \rightarrow 2s^22p^5 [^2P_{3/2}]$ and $(2s2p^6 [^2S_{1/2}]6s)_{J=1} \rightarrow 2s2p^6 [^2S_{1/2}]$.

F-like Ni^{19+} (MR = $\{2s^22p^5, 2s2p^6, 2s^22p^43p, 2s2p^53p\}$)			
AO	$E(2s^22p^5 [^2P_{3/2}])$	$E(2s2p^6 [^2S_{1/2}])$	$\Delta E(2s2p^6 [^2S_{1/2}] \rightarrow 2s^22p^5 [^2P_{3/2}])$
{3s, 3p, 3d}	-1292.5833877	-1287.0299079	151.118
{4s, 4p, 4d, 4f}	-1292.7902178	-1287.3083550	149.169
{5s, 5p, 5d, 5f, 5g}	-1292.8534402	-1287.3745748	149.088
{6s, 6p, 6d, 6f, 6g, 6h}	-1292.8806642	-1287.4035955	149.039
{7s, 7p, 7d, 7f, 7g, 7h, 7i}	-1292.9096358	-1287.4331842	149.022
{8s, 8p, 8d, 8f, 8g, 8h, 8i, 8k}	-1292.9238447	-1287.4474401	149.020
{9s, 9p, 9d, 9f, 9g, 9h, 9i, 9k}	-1292.9295149	-1287.4531798	149.019
Ne-like Ni^{18+} (MR = $\{2s2p^65s, 2s2p^66s, 2s2p^67s\}$)			
AO	$E((2s2p^6 [^2S_{1/2}]6s)_{J=1})$	$\Delta E((2s2p^6 [^2S_{1/2}]6s)_{J=1} \rightarrow 2s2p^6 [^2S_{1/2}])$	
{8s, 8p, 8d, 8f, 8g, 8h, 8i, 8k}	-1292.8391704		158.08
{9s, 9p, 9d, 9f, 9g, 9h, 9i, 9k}	-1292.8712688		151.37
{10s, 10p, 10d, 10f, 10g, 10h, 10i, 10k}	-1292.8918299		150.13
{11s, 11p, 11d, 11f, 11g, 11h, 11i, 10k}	-1292.9022762		149.63
{12s, 12p, 12d, 12f, 12g, 12h, 11i, 10k}	-1292.9085850		148.99
{13s, 13p, 13d, 13f, 13g, 12h, 11i, 10k}	-1292.9165405		148.82
{14s, 14p, 14d, 14f, 13g, 12h, 11i, 10k}	-1292.9277362		148.97

as

$$H_0 = \int d^3x \psi^\dagger(x) [-i\boldsymbol{\alpha}\nabla + \beta m + V_C(\mathbf{x}) + V_{\text{scr}}(\mathbf{x})] \psi(x), \quad (15)$$

where α_i and β are the Dirac matrices, $\psi(x)$ is a field operator expanded in terms of the Dirac wave functions $\psi_n(\mathbf{x})$:

$$[-i\boldsymbol{\alpha}\nabla + \beta m + V_C(\mathbf{x}) + V_{\text{scr}}(\mathbf{x})] \psi_n(\mathbf{x}) = \varepsilon_n \psi_n(\mathbf{x}). \quad (16)$$

In Eq. (15), in addition to the nuclear Coulomb potential V_C the screening potential V_{scr} which partially accounts for the interelectronic interaction has been added. In our calculations, we employ the core-Hartree and Kohn-Sham potentials.

The perturbation expansion is performed with respect to the interaction Hamiltonian

$$H_{\text{int}} = \int d^3x [\bar{\psi}(x) e\gamma^\mu A_\mu(x) \psi(x) - \psi^\dagger(x) V_{\text{scr}}(\mathbf{x}) \psi(x)], \quad (17)$$

where $\gamma^\mu = (\beta, \beta\alpha_i)$, $A_\mu(x)$ is a photon field operator. The second term in Eq. (17) corresponds to the subtraction of the counterterm. For constructing the perturbative expansion, we use the two-time Green function method [75]. In the present calculations, we account entirely for the first-order corrections, which are given by the one-photon exchange and the one-electron self-energy and vacuum polarization diagrams. These diagrams are computed employing the well-known formal expressions, which can be found in, e.g., Refs. [75, 76]. The second-order diagrams include the many-electron radiative (so-called screened QED), one-electron two-loop, and two-photon exchange corrections. Here, we evaluate only the screened QED correction employing the techniques and methods thoroughly presented in Refs. [71, 77–79]. For

the one-electron two-loop contribution, we use the hydrogenic values from Ref. [80]. While the two-photon exchange diagrams are taken into account within the Breit approximation, and the uncertainty from missing higher-order correction is estimated to be $\alpha/(8\pi)(\alpha Z)^4/Z^2$ multiplied by a factor 5.

The terms which were not accounted for by the rigorous QED theory have been evaluated within the Breit approximation employing the configuration-interaction Dirac-Fock-Strum (CI-DFS) method [81–83]. Within this method, the many-electron wave-function and the energy of an atom E in the Breit approximation are to be found as solutions of the Dirac-Coulomb-Breit Hamiltonian. Thus, the CI-DFS method is used to calculate the second and higher orders interelectronic-interaction corrections. Moreover, we have evaluated the recoil correction employing the many-body relativistic mass shift Hamiltonian [77, 84, 85].

IV. RESULTS AND DISCUSSION

The fitted curve of the low-energy DR spectrum is presented in FIG. 7 (a). The data points below 10 meV are not included in the fitting due to the inevitable rate coefficient enhancement [22, 46, 55, 56]. In the fitting procedure, the first resonance was treated as a Lorentzian profile multiplied by a factor of E_{res}/E while the other ones are regarded as delta functions. According to the curve fitting, the first resonance was determined to be at 86 meV with an uncertainty of less than 2 meV. The fitted resonance width and strength are also found in agreement with the FAC calculation. To elucidate the isolated DR resonances more clearly, the fitted DR resonances are compared with the background subtracted experimental

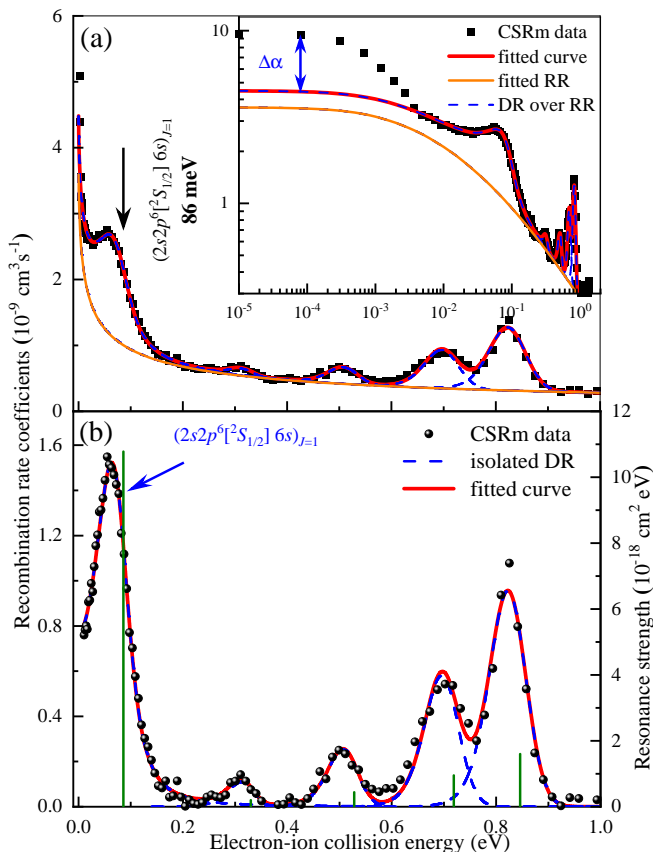


FIG. 7. (a) The fitted curve for the low-energy DR spectrum. The dots are the measured data while the red solid line is the fitted curve, including the continuous RR background (orange solid line) and the isolated DR resonances (blue dashed lines). It should be noted that the DR resonances are superimposed on the RR background. $\Delta\alpha$ denotes the rate coefficient enhancement at near-zero collision energies. (b) The RR and background-subtracted DR rate coefficients along with the fitted curves. The green column bars represent the fitted DR resonance positions and strengths.

data in FIG. 7 (b). The electron beam temperatures obtained from the fitting are $k_B T_{\parallel} = 0.56(0.05)$ meV and $k_B T_{\perp} = 23(1)$ meV. The total uncertainty on the determination of the first DR resonance position is less than 4 meV.

The $6s$ binding energy in the $(2s2p^6[{}^2S_{1/2}]6s)_{J=1}$ state is calculated by the MCDHF and stabilization methods, respectively. The large scale MCDHF calculations do not really evaluate convergent binding energy increasing active set. Note that the energy of the autoionizing state is extremely sensitive to the basis chosen due to the degeneration with continuum states. An estimated error on the calculated binding energy is around 10 meV. In addition, the binding energy has also been calculated by using the stabilization method. For the transition $2s2p^66s[{}^3S_1] - 2s^22p^6[{}^1S_0]$ energy we get 148.946(6) eV. Combining the calculated $6s$ binding energy in the $(2s2p^6[{}^2S_{1/2}]6s)_{J=1}$ state and the experimentally derived

DR resonance position, the $2s^22p^5[{}^2P_{1/2}] \rightarrow 2s2p^6[{}^2S_{1/2}]$ transition energy in fluorine-like nickel are listed in Table III.

TABLE III. Comparison of the experimental and theoretical results for the transition $2s^22p^5[{}^2P_{1/2}] \rightarrow 2s2p^6[{}^2S_{1/2}]$ energy in fluorine-like nickel ion (in eV).

Method	Energy (eV)
Experiment + theory	
Exp. + MCDHF	149.056(4) _{exp} (10) _{theo}
Exp. + SM	149.032(4) _{exp} (6) _{theo}
Theory	
MCDHF	149.019(10)
<i>Ab initio</i>	149.046(7)

Moreover, the $2s^22p^5[{}^2P_{1/2}] \rightarrow 2s2p^6[{}^2S_{1/2}]$ transition energy has also calculated in the frame of fully relativistic MCDHF method and *ab initio* QED approach. The calculated transition energies are also presented in Table III. The large scale MCDHF calculation yields convergent values with the increasing size of active set and the estimated uncertainty on the calculated binding energy is 10 meV according to the convergence. In the *ab initio* QED calculation, the zeroth-order Dirac result is extended by the correlation corrections evaluated within the Breit approximation, by the first- and second-order QED contributions, as well as by the recoil term. Calculations were performed employing two starting potentials, core-Hartree and Kohn-Sham. The final results as presented in Table IV appear to be independent of the initial potential. In Table IV, we present the individual theoretical contributions to the transition $2s^22p^5[{}^2P_{1/2}] \rightarrow 2s2p^6[{}^2S_{1/2}]$ energy in fluorine-like nickel calculated as has been explained above in both utilized screening potentials. As one can see from the table the total results in both potentials perfectly agree with each other. The final uncertainty is dominated by the estimation of the QED effect for the two-photon exchange correction.

TABLE IV. Individual contributions to the transition $2s^22p^5[{}^2P_{1/2}] \rightarrow 2s2p^6[{}^2S_{1/2}]$ energy in fluorine-like nickel ion (in eV).

Contribution	Core-Hartree	Kohn-Sham
Dirac	123.911	128.743
Correlation (1)	27.190	22.723
Correlation (2)	-1.536	-1.972
Correlation (3)	0.032(2)	0.102(2)
QED (1)	-0.506	-0.510
QED (2)	-0.033(6)	-0.028(6)
Recoil	-0.012(3)	-0.012(3)
Total	149.046(7)	149.046(7)

The derived transition energies are compared with the available theoretical calculations and experimental observations in Figure 8. The determined transition energies agree with the most accurate plasma observation

[35] within the error bars. The calculated data by the SuperStructure code [86] and the coupled cluster method with single and double excitations (CCSD) [40] are found much larger than the experimental data. The MBPT [36, 37] and MCDHF [37] calculations report values for the transition energies without uncertainties, what hampers the accurate comparison. The value obtained within the CI-MCDF method [38] agrees well with our both results experimental and theoretical within given error bars, but our values are more precise. The individual contributions in Table IV indicate that the third-order correlation can contribute 0.032(2) eV to the total transition energy. In the calculations where the correlation effect was handled with care [36–38], the yielded values agree better with the experimental data. The MBPT calculations [36, 37] are found lower than the present data indicating that the many-body expansion in many-electron systems remains a challenge task.

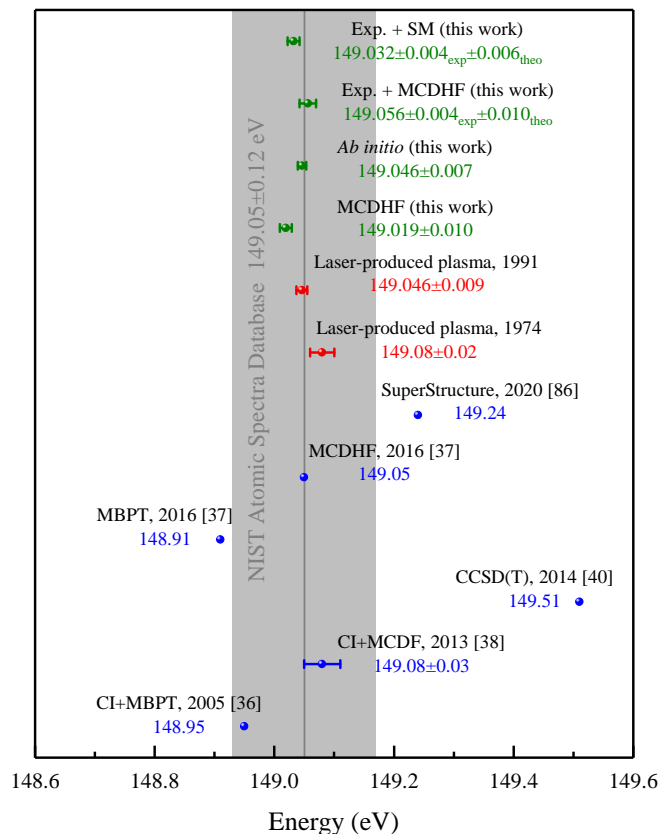


FIG. 8. Available experimental and theoretical transition energy of the $2s^2 2p^5 [^2P_{1/2}] \rightarrow 2s 2p^6 [^2S_{1/2}]$ along with the present experimental derived data and theoretical calculations.

V. SUMMARY AND OUTLOOK

Electron-ion recombination rate coefficients of fluorine-like nickel ions have been measured at the heavy-ion stor-

age ring CSRm by employing the merged-beam method. The measured rate coefficients agree well with the most recent theoretical calculation by the FAC code, even at very low collision energies. The level-resolved theoretical calculation assists the identification of the measured DR resonances, in which the first isolated resonance is recognized as the recombination channel via the $(2s 2p^6 [^2S_{1/2}] 6s)_{J=1}$ intermediate state. By fitting the measured recombination spectra, the collision energy for the first resonance is determined to be 86 meV, with a systemic uncertainty of 2 meV and a fitting error of 2 meV. The accurate measurement of the resonant position enables a precise determination of the associate $2s^2 2p^5 [^2P_{1/2}] \rightarrow 2s 2p^6 [^2S_{1/2}]$ transition energy.

To determine the transition energy, the MCDHF and stabilization methods are employed to calculate the $6s$ binding energy in the $(2s 2p^6 [^2S_{1/2}] 6s)_{J=1}$ intermediate state. The large scale MCDHF calculation does not generate convergent binding energies due to the fact that the autoionizing state is degenerated with the continuum states and the energy level is extremely sensitive to the basis chosen. The derived $2s^2 2p^5 [^2P_{1/2}] \rightarrow 2s 2p^6 [^2S_{1/2}]$ transition energies are $149.056(4)_{\text{exp}}(10)_{\text{MCDHF}}$ and $149.032(4)_{\text{exp}}(6)_{\text{SM}}$, respectively. The both data agree with the most accurate plasma observation. Furthermore, the transition energy has also been calculated by the fully relativistic MCDHF and *ab initio* QED approaches. Detailed implementation of individual contributions to the transition energy indicates that higher order correlation and QED effects contribute prominently.

This work is the first precision DR spectroscopy with highly charged ions at the CSRm. The study not only provides an opportunity to test QED and correlation effects in many-electron systems but also paves the way for future precision studies with highly-charged ions at the CSRm and HIAF.

ACKNOWLEDGMENTS

This work has been funded by the National Key R&D Program of China under Grant No. 2017YFA0402300; the National Natural Science Foundation of China through Grants No. U1932207, No. 11904371, No. 11674066, and No. 12104437, the Strategic Priority Research Program of Chinese Academy of Sciences Grant No. XDB34020000, and the Heavy Ion Research Facility in Lanzhou (HIRFL). S.X.W. is grateful to the Natural Science Foundation of Anhui Province (Grant No. 2108085QA27), and the Fundamental Research Funds for the Central Universities. W.Q.W. thanks the support from the Youth Innovation Promotion Association of the Chinese Academy of Sciences. A.V.V. acknowledges financial support by the Government of the Russian Federation through the ITMO Fellowship and Professorship Program. The authors would like to thank the CSR accelerator staff for their technical support during the

experiment.

-
- [1] M. S. Safronova, D. Budker, D. DeMille, D. F. J. Kimball, A. Derevianko, and C. W. Clark, *Rev. Mod. Phys.* **90**, 025008 (2018).
- [2] M. G. Kozlov, M. S. Safronova, J. R. Crespo López-Urrutia, and P. O. Schmidt, *Rev. Mod. Phys.* **90**, 045005 (2018).
- [3] P. Indelicato, *J. Phys. B: At. Mol. Opt. Phys.* **52**, 232001 (2019).
- [4] P. Beiersdorfer, *Can. J. Phys.* **87**, 9 (2009).
- [5] P. Beiersdorfer, *J. Phys. B: At. Mol. Opt. Phys.* **43**, 074032 (2010).
- [6] S. Schippers, *Nucl. Instrum. Methods Phys. Res. Sec. B* **267**, 192 (2009), proceedings of the Fourth International Conference on Elementary Processes in Atomic Systems.
- [7] M. Steck and Y. A. Litvinov, *Prog. Part. Nucl. Phys.* **115**, 103811 (2020).
- [8] P. Indelicato, *J. Phys. B: At. Mol. Opt. Phys.* **52**, 232001 (2019).
- [9] E. Lindroth, H. Danared, P. Glans, Z. Pešić, M. Tokman, G. Viktor, and R. Schuch, *Phys. Rev. Lett.* **86**, 5027 (2001).
- [10] T. Stöhlker, P. H. Mokler, K. Beckert, F. Bosch, H. Eickhoff, B. Franzke, M. Jung, Y. Kandler, O. Klepper, C. Kozhuharov, R. Moshhammer, F. Nolden, H. Reich, P. Rymuza, P. Spädtke, and M. Steck, *Phys. Rev. Lett.* **71**, 2184 (1993).
- [11] J. R. Crespo López-Urrutia, P. Beiersdorfer, D. W. Savin, and K. Widmann, *Phys. Rev. Lett.* **77**, 826 (1996).
- [12] P. Beiersdorfer, A. L. Osterheld, J. H. Scofield, J. R. Crespo López-Urrutia, and K. Widmann, *Phys. Rev. Lett.* **80**, 3022 (1998).
- [13] T. Stöhlker, P. H. Mokler, F. Bosch, R. W. Dunford, F. Franzke, O. Klepper, C. Kozhuharov, T. Ludziejewski, F. Nolden, H. Reich, P. Rymuza, Z. Stachura, M. Steck, P. Swiat, and A. Warczak, *Phys. Rev. Lett.* **85**, 3109 (2000).
- [14] M. Lestinsky, E. Lindroth, D. A. Orlov, E. W. Schmidt, S. Schippers, S. Böhm, C. Brandau, F. Sprenger, A. S. Terekhov, A. Müller, and A. Wolf, *Phys. Rev. Lett.* **100**, 033001 (2008).
- [15] R. A. Phaneuf, C. C. Havener, G. H. Dunn, and A. Müller, *Rep. Prog. Phys.* **62**, 1143 (1999).
- [16] S. Schippers, *Nucl. Instrum. Methods B* **350**, 61 (2015).
- [17] C. Brandau, C. Kozhuharov, M. Lestinsky, A. Müller, S. Schippers, and T. Stöhlker, *Phys. Scr.* **T166**, 014022 (2015).
- [18] R. Schuch and S. Böhm, *J. Phys. Conf. Ser.* **88**, 012002 (2007).
- [19] Z. K. Huang, W. Q. Wen, H. B. Wang, X. Xu, L. F. Zhu, X. Y. Chuai, Y. J. Yuan, X. L. Zhu, X. Y. Han, L. J. Mao, J. Li, X. M. Ma, T. L. Yan, J. C. Yang, G. Q. Xiao, J. W. Xia, and X. Ma, *Phys. Scr.* **T166**, 014023 (2015).
- [20] Z. K. Huang, W. Q. Wen, X. Xu, S. Mahmood, S. X. Wang, H. B. Wang, L. J. Dou, N. Khan, N. R. Badnell, S. P. Preval, S. Schippers, T. H. Xu, Y. Yang, K. Yao, W. Q. Xu, X. Y. Chuai, X. L. Zhu, D. M. Zhao, L. J. Mao, X. M. Ma, J. Li, R. S. Mao, Y. J. Yuan, B. Wu, L. N. Sheng, J. C. Yang, H. S. Xu, L. F. Zhu, and X. Ma, *Astrophys. J. Suppl. Ser.* **235**, 2 (2018).
- [21] S. X. Wang, X. Xu, Z. K. Huang, W. Q. Wen, H. B. Wang, N. Khan, S. P. Preval, N. R. Badnell, S. Schippers, S. Mahmood, L. J. Dou, X. Y. Chuai, D. M. Zhao, X. L. Zhu, L. J. Mao, X. M. Ma, J. Li, R. S. Mao, Y. J. Yuan, M. T. Tang, D. Y. Yin, J. C. Yang, X. Ma, and L. F. Zhu, *Astrophys. J.* **862**, 134 (2018).
- [22] S.-X. Wang, Z.-K. Huang, W.-Q. Wen, C.-Y. Chen, S. Schippers, X. Xu, S. Sardar, N. Khan, H.-B. Wang, L.-J. Dou, S. Mahmood, D.-M. Zhao, X.-L. Zhu, L.-J. Mao, X.-M. Ma, J. Li, M.-T. Tang, R.-S. Mao, D.-Y. Yin, Y.-J. Yuan, J.-C. Yang, Y.-L. Shi, C.-Z. Dong, X.-W. Ma, and L.-F. Zhu, *A&A* **627**, A171 (2019).
- [23] Z. K. Huang, W. Q. Wen, S. X. Wang, N. Khan, H. B. Wang, C. Y. Chen, C. Y. Zhang, S. P. Preval, N. R. Badnell, W. L. Ma, X. Liu, D. Y. Chen, X. L. Zhu, D. M. Zhao, L. J. Mao, X. M. Ma, J. Li, M. T. Tang, R. S. Mao, D. Y. Yin, W. Q. Yang, J. C. Yang, Y. J. Yuan, L. F. Zhu, and X. Ma, *Phys. Rev. A* **102**, 062823 (2020).
- [24] W. Q. Wen, Z. K. Huang, S. X. Wang, N. Khan, H. B. Wang, C. Y. Chen, C. Y. Zhang, S. Preval, N. R. Badnell, W. L. Ma, D. Y. Chen, X. Liu, D. M. Zhao, L. J. Mao, J. Li, X. M. Ma, M. T. Tang, D. Y. Yin, W. Q. Yang, Y. J. Yuan, J. C. Yang, L. F. Zhu, and X. Ma, *Astrophys. J.* **905**, 36 (2020).
- [25] N. Khan, Z.-K. Huang, W.-Q. Wen, S.-X. Wang, C.-Y. Chen, C.-Y. Zhang, H.-B. Wang, X. Liu, W.-L. Ma, D.-Y. Chen, K. Yao, D.-M. Zhao, L.-J. Mao, X.-M. Ma, J. Li, M.-T. Tang, D.-Y. Yin, Y.-J. Yuan, J.-C. Yang, L.-F. Zhu, and X.-W. Ma, *J. Phys. B: At. Mol. Opt. Phys.* **55**, 035001 (2022).
- [26] S. Madzunkov, E. Lindroth, N. Eklöv, M. Tokman, A. Paál, and R. Schuch, *Phys. Rev. A* **65**, 032505 (2002).
- [27] S. Kieslich, S. Schippers, W. Shi, A. Müller, G. Gwinner, M. Schnell, A. Wolf, E. Lindroth, and M. Tokman, *Phys. Rev. A* **70**, 042714 (2004).
- [28] D. A. Orlov, C. Krantz, D. Bernhardt, C. Brandau, J. Hoffmann, A. Müller, T. Ricsóka, S. Schippers, A. Shornikov, and A. Wolf, *J. Phys. Conf. Ser.* **163**, 012058 (2009).
- [29] C. Krantz, D. A. Orlov, D. Bernhardt, C. Brandau, J. Hoffmann, A. Müller, T. Ricsóka, S. Ricz, S. Schippers, and A. Wolf, *J. Phys. Conf. Ser.* **163**, 012059 (2009).
- [30] C. Brandau, C. Kozhuharov, A. Müller, W. Shi, S. Schippers, T. Bartsch, S. Böhm, C. Böhme, A. Hoffknecht, H. Knopp, N. Grün, W. Scheid, T. Steih, F. Bosch, B. Franzke, P. H. Mokler, F. Nolden, M. Steck, T. Stöhlker, and Z. Stachura, *Phys. Rev. Lett.* **91**, 073202 (2003).
- [31] D. Bernhardt, C. Brandau, Z. Harman, C. Kozhuharov, S. Böhm, F. Bosch, S. Fritzsche, J. Jacobi, S. Kieslich, H. Knopp, F. Nolden, W. Shi, Z. Stachura, M. Steck, T. Stöhlker, S. Schippers, and A. Müller, *Phys. Rev. A* **91**, 012710 (2015).
- [32] M. F. Gu, *Can. J. Phys.* **86**, 675 (2008).
- [33] G. Doschek, U. Feldman, R. Cowan, and L. Cohen, *Astrophys. J.* **188**, 417 (1974).

- [34] C. Breton, C. D. Michelis, M. Finkenthal, and M. Mattioli, *J. Opt. Soc. Am.* **69**, 1652 (1979).
- [35] J. Sugar, V. Kaufman, and W. L. Rowan, *J. Opt. Soc. Am. B* **9**, 344 (1992).
- [36] M. F. Gu, *At. Data Nucl. Data Tables* **89**, 267 (2005).
- [37] R. Si, S. Li, X. L. Guo, Z. B. Chen, T. Brage, P. Jönsson, K. Wang, J. Yan, C. Y. Chen, and Y. M. Zou, *Astrophys. J. Suppl. Ser.* **227**, 16 (2016).
- [38] P. Jönsson, A. Alkauskas, and G. Gaigalas, *At. Data Nucl. Data Tables* **99**, 431 (2013).
- [39] C. J. Fontes and H. L. Zhang, *At. Data Nucl. Data Tables* **113**, 293 (2017).
- [40] Nandy, D. K. and Sahoo, B. K., *A&A* **563**, A25 (2014).
- [41] A. Kramida, Yu. Ralchenko, J. Reader, and and NIST ASD Team, NIST Atomic Spectra Database (ver. 5.8), [Online]. Available: <https://physics.nist.gov/asd> [2021, July 20]. National Institute of Standards and Technology, Gaithersburg, MD. (2020).
- [42] X. Xu, S.-X. Wang, Z.-K. Huang, W.-Q. Wen, H.-B. Wang, T.-H. Xu, X.-Y. Chuai, L.-J. Dou, W.-Q. Xu, C.-Y. Chen, C.-Y. Li, J.-G. Wang, Y.-L. Shi, C.-Z. Dong, L.-J. Mao, D.-Y. Yin, J. Li, X.-M. Ma, J.-C. Yang, Y.-J. Yuan, X.-W. Ma, and L.-F. Zhu, *Chin. Phys. B* **27**, 063402 (2018).
- [43] N. Khan, Z.-K. Huang, W.-Q. Wen, S. Mahmood, L.-J. Dou, S.-X. Wang, X. Xu, H.-B. Wang, C.-Y. Chen, X.-Y. Chuai, X.-L. Zhu, D.-M. Zhao, L.-J. Mao, J. Li, D.-Y. Yin, J.-C. Yang, Y.-J. Yuan, L.-F. Zhu, and X.-W. Ma, *Chin. Phys. C* **42**, 064001 (2018).
- [44] Z. Huang, S. Wang, W. Wen, X. Xu, H. Wang, S. Li, L. Dou, N. Khan, S. Mahmood, X. Zhu, D. Zhao, L. Mao, X. Ma, J. Li, R. Mao, J. Yang, D. Yin, Y. Yuan, C. Chen, L. Zhu, and X. Ma, *X-Ray Spectrometry* **49**, 155 (2020).
- [45] S. Mahmood, Z. K. Huang, W. Q. Wen, S. X. Wang, C. Y. Chen, N. Khan, X. Xu, L. J. Dou, H. B. Wang, X. L. Zhu, D. M. Zhao, L. J. Mao, X. M. Ma, J. Li, M. T. Tang, R. S. Mao, W. Q. Yang, D. Y. Yin, Y. J. Yuan, J. C. Yang, L. F. Zhu, and X. Ma, *J. Phys. B: At. Mol. Opt. Phys.* **53**, 085004 (2020).
- [46] N. Khan, Z.-K. Huang, W.-Q. Wen, S.-X. Wang, H.-B. Wang, W.-L. Ma, X.-L. Zhu, D.-M. Zhao, L.-J. Mao, J. Li, X.-M. Ma, M.-T. Tang, D.-Y. Yin, W.-Q. Yang, J.-C. Yang, Y.-J. Yuan, L.-F. Zhu, and X.-W. Ma, *Chin. Phys. B* **29**, 033401 (2020).
- [47] H. W. Zhao, L. T. Sun, J. W. Guo, W. Lu, D. Z. Xie, D. Hitz, X. Z. Zhang, and Y. Yang, *Phys. Rev. Accel. Beams* **20**, 094801 (2017).
- [48] H. Danared, *Nucl. Instrum. Methods A* **335**, 397 (1993).
- [49] G. Kilgus, D. Habs, D. Schwalm, A. Wolf, N. R. Badnell, and A. Müller, *Phys. Rev. A* **46**, 5730 (1992).
- [50] V. Bocharov, A. Bublely, Y. Boimelstein, V. Vere-meenko, V. Voskoboinikov, A. Goncharov, V. Grishanov, A. Dranichnikov, Y. Evtushenko, N. Zapitkin, M. Zakhvatkin, A. Ivanov, V. Kokoulin, V. Kolmogorov, M. Kondaurov, E. Konstantinov, S. Konstantinov, G. Krainov, A. Kriuchkov, E. Kuper, A. Medvedko, L. Mironenko, V. Panasiuk, V. Parkhomchuk, S. Petrov, V. Reva, P. Svishev, B. Skarbo, B. Smirnov, B. Sukhina, M. Tiunov, V. Shirokov, K. Shrainer, X. Yang, H. Zhao, Z. Wang, J. Li, J. Zhang, W. Zhang, H. Yan, H. Yan, and G. Xia, *Nucl. Instrum. Methods A* **532**, 144 (2004).
- [51] H. Poth, *Phys. Rep.* **196**, 135 (1990).
- [52] W. Wen, X. Ma, W. Xu, L. Meng, X. Zhu, Y. Gao, S. Wang, P. Zhang, D. Zhao, H. Liu, L. Zhu, X. Yang, J. Li, X. Ma, T. Yan, J. Yang, Y. Yuan, J. Xia, H. Xu, and G. Xiao, *Nucl. Instrum. Methods B* **317**, 731 (2013).
- [53] J. Wu, Y. Zang, F. Nolden, M. Sanjari, P. Hülsmann, F. Caspers, T. Zhao, M. Li, J. Zhang, J. Li, Y. Zhang, G. Zhu, S. Zhang, X. Ma, H. Xu, J. Yang, J. Xia, R. Mao, and P. Petri, *Nucl. Instrum. Methods B* **317**, 623 (2013).
- [54] D. Bernhardt, C. Brandau, Z. Harman, C. Kozhuharov, A. Müller, W. Scheid, S. Schippers, E. W. Schmidt, D. Yu, A. N. Artemyev, I. I. Tupitsyn, S. Böhm, F. Bosch, F. J. Currell, B. Franzke, A. Gumberidze, J. Jacobi, P. H. Mokler, F. Nolden, U. Spillman, Z. Stachura, M. Steck, and T. Stöhlker, *Phys. Rev. A* **83**, 020701 (2011).
- [55] G. Gwinner, A. Hoffknecht, T. Bartsch, M. Beutelspacher, N. Eklöw, P. Glans, M. Grieser, S. Krohn, E. Lindroth, A. Müller, A. A. Saghir, S. Schippers, U. Schramm, D. Schwalm, M. Tokman, G. Wissler, and A. Wolf, *Phys. Rev. Lett.* **84**, 4822 (2000).
- [56] C. Heerlein, G. Zwicknagel, and C. Toepffer, *Phys. Rev. Lett.* **89**, 083202 (2002).
- [57] W. Shi, T. Bartsch, C. Böhme, C. Brandau, A. Hoffknecht, H. Knopp, S. Schippers, A. Müller, C. Kozhuharov, K. Beckert, F. Bosch, B. Franzke, P. H. Mokler, F. Nolden, M. Steck, T. Stöhlker, and Z. Stachura, *Phys. Rev. A* **66**, 022718 (2002).
- [58] C. Froese Fischer, G. Gaigalas, P. Jönsson, and J. Bieroń, *Comput. Phys. Commun.* **237**, 184 (2019).
- [59] I. P. Grant, *Relativistic Quantum Theory of Atoms and Molecules: Theory and Computation* (Springer-Verlag, New York, 2007).
- [60] J. P. Desclaux, *Comput. Phys. Commun.* **9**, 31 (1975).
- [61] Y. K. Ho, *Phys. Rep.* **99**, 1 (1983).
- [62] B. I. Schneider, *J. Phys.: Conf. Ser.* **759**, 012002 (2016).
- [63] A. U. Hazi and H. S. Taylor, *Phys. Rev. A* **1**, 1109 (1970).
- [64] M. F. Fels and A. U. Hazi, *Phys. Rev. A* **4**, 662 (1971).
- [65] J. Müller, X. Yang, and J. Burgdörfer, *Phys. Rev. A* **49**, 2470 (1994).
- [66] S. Kar and Y. K. Ho, *Phys. Rev. A* **72**, 010703 (2005).
- [67] J. K. Saha and T. K. Mukherjee, *Phys. Rev. A* **80**, 022513 (2009).
- [68] P. Amaro, J. P. Santos, S. Bhattacharyya, T. K. Mukherjee, and J. K. Saha, *Phys. Rev. A* **103**, 012811 (2021).
- [69] V. A. Mandelshtam, T. R. Ravuri, and H. S. Taylor, *Phys. Rev. Lett.* **70**, 1932 (1993).
- [70] W. H. Furry, *Phys. Rev.* **81**, 115 (1951).
- [71] A. V. Volotka, M. Bilal, R. Beerwerth, X. Ma, T. Stöhlker, and S. Fritzsche, *Phys. Rev. A* **100**, 010502 (2019).
- [72] V. M. Shabaev, I. I. Tupitsyn, M. Y. Kaygorodov, Y. S. Kozhedub, A. V. Malyshev, and D. V. Mironova, *Phys. Rev. A* **101**, 052502 (2020).
- [73] G. O'Neil, S. Sanders, P. Szypryt, Dipti, A. Gall, Y. Yang, S. M. Brewer, R. Doriase, J. Fowler, A. Naing, D. Swetz, J. Tan, J. Ullom, A. V. Volotka, E. Takacs, and Y. Ralchenko, *Phys. Rev. A* **102**, 032803 (2020).
- [74] Q. Lu, C. L. Yan, G. Q. Xu, N. Fu, Y. Yang, Y. Zou, A. V. Volotka, J. Xiao, N. Nakamura, and R. Hutton, *Phys. Rev. A* **102**, 042817 (2020).
- [75] V. M. Shabaev, *Phys. Rep.* **356**, 119 (2002).
- [76] P. J. Mohr, G. Plunien, and G. Soff, *Phys. Rep.* **293**, 227 (1998).
- [77] Y. S. Kozhedub, A. V. Volotka, A. N. Artemyev, D. A. Glazov, G. Plunien, V. M. Shabaev, I. I. Tupitsyn, and T. Stöhlker, *Phys. Rev. A* **81**, 042513 (2010).
- [78] A. V. Malyshev, A. V. Volotka, D. A. Glazov, I. I. Tupit-

- syn, V. M. Shabaev, and G. Plunien, *Phys. Rev. A* **90**, 062517 (2014).
- [79] A. V. Malyshev, A. V. Volotka, D. A. Glazov, I. I. Tupitsyn, V. M. Shabaev, and G. Plunien, *Phys. Rev. A* **92**, 012514 (2015).
- [80] V. A. Yerokhin and V. M. Shabaev, *J. Phys. Chem. Ref. Data* **44**, 033103 (2015).
- [81] I. I. Tupitsyn, V. M. Shabaev, J. R. Crespo López-Urrutia, I. Draganić, R. Soria Orts, and J. Ullrich, *Phys. Rev. A* **68**, 022511 (2003).
- [82] I. I. Tupitsyn, A. V. Volotka, D. A. Glazov, V. M. Shabaev, G. Plunien, J. R. Crespo López-Urrutia, A. Lapierre, and J. Ullrich, *Phys. Rev. A* **72**, 062503 (2005).
- [83] M. Y. Kaygorodov, Y. S. Kozhedub, I. I. Tupitsyn, A. V. Malyshev, D. A. Glazov, G. Plunien, and V. M. Shabaev, *Phys. Rev. A* **99**, 032505 (2019).
- [84] C. W. P. Palmer, *J. Phys. B* **20**, 5987 (1987).
- [85] V. M. Shabaev and A. N. Artemyev, *J. Phys. B* **27**, 1307 (1994).
- [86] G. Celik, S. Ates, and S. N. Nahar, *Ind. J. Phys.* **94**, 565 (2020).